Strojniški vestnik - Journal of Mechanical Engineering 70(2024)3-4, pp1-pp13
Received for review: XXXX
Received revised form: XXXX
Accepted for publication: XXXX
DOI:10.5545/sv-jme.2023.673
Original Scientific Paper

Service Performance Optimization and Experimental Study of a New W-W Type Non-circular Planetary Gear Train

Changbin Dong[1]— Xudong Yang[1]—Dawei Li[1] —Gang Zhao[2]—Anran Wan[3]—Yongping Liu[1]—Junhai Guo[1]

1 Lanzhou University of Technology, School of Mechanical and Electrical Engineering, China
2 Wuhan University of Science and Technology, Hubei Key Laboratory of Mechanical Transmission and Manufacturing Engineering, China
3 Wuxi Institute of Technology, School of Mechanical Technology

To address the vibration problem in traditional W-W-type non-circular planetary gear trains during operation, this study proposes two new combinations of W-W-type non-circular planetary gear trains. The study focuses on analysing the transmission error and improving service performance. By utilizing the conjugate theory and the coordinate transformation theory, an accurate mathematical model for non-circular gears is derived. The transmission error models for the two combination forms of the non-circular planetary gear train are established using the incremental meshing line method. The analysis also examines the influence of eccentricity on the transmission error. Kinematic analysis of the multi-body dynamics model confirms that the new W-W type non-circular planetary gear train, formed by combining non-circular gears and cylindrical gears, exhibits superior transmission performance. Furthermore, a test analysis is conducted on the roller pumping unit test platform and the indicator diagrams of the pumping unit under various working conditions are obtained. The study concludes that the optimal matching mode for the sucker rod counterweight and motor frequency of the reversing device of the pumping unit is 20 kN and 20 Hz, and the dynamic balance of the pumping unit load can be achieved by adjusting the motor frequency.

Keywords: Non-circular planetary gear train, reversing device, incremental meshing line method, transmission error, indicator diagram

Highlights

- *Two new W-W type non-circular planetary gear train combinations have been proposed to reduce torque fluctuations at the output end.*
- *A new method for establishing the transmission error model of new W-W-type non-circular gear planetary gear trains based on the incremental meshing line method was proposed.*
- *An idealized indoor pumping unit test platform was built, and indicator diagrams of non-circular gear pumping units under different working conditions are obtained.*

0 INTRODUCTION

As a new type of gear transmission, non-circular gear (NCG) is mainly used to realize nonlinear rotation between two transmission shafts [1]. It has the advantages of strong bearing capacity and variable ratio transmission [2] to [4] and is widely used in agriculture, military, aerospace, and other important places. This kind of functional gear device has also evolved in nature [5]. Burrows have found a natural gear structure on the hind legs of the jumping Issus worm. Its distribution type, transmission mode, and functions are consistent with those of NCG, which proves that NCG can also play a functional role in the natural behaviour of jumping insects as a biological gear. With the development of modern machinery towards high speed, heavy load, and high precision, it has been difficult to make a single NCG pair to meet the application requirements. Thanks to the time-varying transmission characteristics of NCG, various transmission forms can be realized by combining different types of NCG into multiple non-circular planetary gear trains (NCPGT), which are applied in hydraulic motors, hydraulic pumps, astronomical clocks, automobile gearboxes, and other fields [6] to [8].

Generally, NCPGT [9] and [10] has four types, namely N-G-W, N-W, W-W, N-N, and each type can achieve different functions and can be applied in different situations. In large-scale agricultural machinery with complex movement tracks, such as automatic seedling picking, hole pricking, fertilization, etc., using an NCG rotating mechanism to replace the traditional crank linkage mechanism can make the improved mechanism have smaller inertia, more compact structure, and maintain high motion accuracy when working at medium and high speeds [11] to [13]. Sun et al. [14] proposed the design method of NCPGT in approximate multi pose transplanting mechanism. Zhao et al. [15] and Ye et al. [16] studied the onion automatic seedling delivery mechanism and vegetable rotary seedling taking mechanism of NCPGT. Yu et al. [17] proposed a planetary gear train formed by the combination of incomplete eccentric circular gear and NCG in order to solve the rigid impact of the seedling picking mechanism of the transmission intermittent

*Corr. Author's Address: XXXXXXXXX

planetary gear train. Based on the space "8"-shaped transplanting track, Wang et al. [18] designed a wide narrow row rice bowl seedling transfer mechanism driven by the combination of plane NCG and bevel gear. The NCPGT transfer mechanism can complete the actions of clamping, pulling, holding, and pushing seedlings, which is of great significance for improving the efficiency of agricultural machinery. In addition to agricultural applications, as the key core component of hydraulic motors [19], NCPGT is widely used in metallurgy, mines, and other dangerous working environments to achieve low-speed and high-torque transmission. Considering that NCPGT often uses several planetary gears to share the load, which will cause uneven load distribution and lead to impact and vibration, Lin [20] proposed a new type of double-sided internal meshing NCPGT. The gear train has only one planetary gear, which avoids the problem of uneven load that may occur due to multiple planetary gears.

Due to the accurate variable ratio transmission characteristics of NCG, the planetary gear train composed of NCG and other mechanisms plays an irreplaceable role in many occasions with special motion requirements and force requirements. However, it is difficult to improve the transmission performance of NCPGT. The existing transmission accuracy is only applicable to agricultural machinery, which makes it difficult to meet the use requirements of high-precision occasions, thus restricting the industrial application and development of NCPGT. Therefore, based on the original W-W type NCPGT, this paper proposes a comparative analysis of the two combination modes of the new W-W type NCPGT and applies them to the reversing device of the drum pumping unit. Through the idealized rod production indoor test, the optimal load and motor frequency matching data of the NCPGT pumping unit are obtained, which will lay a theoretical foundation for improving the transmission performance of the NCPGT and promote its industrial application.

1 THE GENERATION MOTION OF CONJUGATE TOOTH PROFILE FOR NCG

Fig. 1 shows the basic principle of using gear shaper cutters as gear cutters to produce NCG. The principle of tooth profile envelope is to ensure the pure rolling of the pitch surface of a pair of NCG, while the instantaneous contact between another cylindrical gear and the pitch surface of this pair of pure rolling NCG ensures the pure rolling relationship.

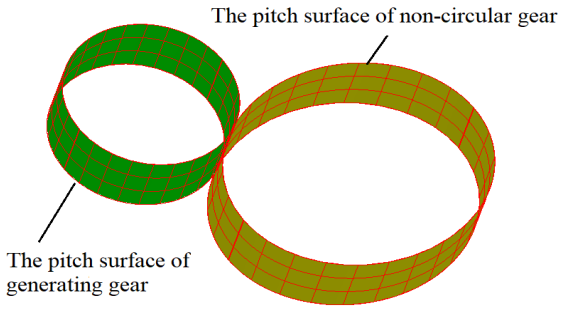

Fig. 1. Basic principle of using cylindrical gear shaper to produce NCGs

The tooth profile of NCG is an involute tooth profile. For involute tooth profile gear transmission, the section of the gear shaping cutter is an involute, and the section equation is:

$$\begin{cases} x_g(u) = r_{gb}(\cos u + u \sin u) \\ y_g(u) = r_{gb}(\sin u - u \cos u) \end{cases}, \quad (1)$$

where $r_{gb}=r_{gp}\cos\alpha$. r_{gb} is the base circle radius. r_{gp} is the indexing circle radius of the gear cutter. u is the tooth shape parameter. Specifically, it is the sum of the unfolding angle and pressure angle of the involute at any point. α is the gear transmission pressure angle.

According to the principle of gear meshing, the relationship between the generating wheel and the generated gear satisfies a pure rolling relationship. Specifically, the pitch curve of the gear shaper and the pitch curve of the NCGs are in instantaneous tangent contact, so the coordinate system can be established through the tangent vector and normal vector of the NCG pitch curve to build the kinematic relationship between the coordinate systems. Based on the basic idea of the motion reversal method, if an NCG is fixed, the relationship between the coordinate system of the gear shaper cutter, the coordinate system of the NCG, and the auxiliary coordinate system at the contact point P of the gear shaper cutter can be defined.

Fig. 2 shows the coordinate conversion relationship when producing NCGs, which contains the following three coordinate systems:

(1) Fixed coordinate system $S_0(O_0-x_0y_0z_0)$, which is fixed on an NCG to be produced. The rotation angle of an NCG is expressed as θ, and the pitch curve equation is defined as $r_p(\theta)$.

(2) Auxiliary coordinate system $S_G(O_g-x_Gy_Gz_G)$, which is determined by the normal and tangential directions of the NCG pitch curve and the contact point P of the generating tool (gear shaper), as well as the center of the generating wheel. The

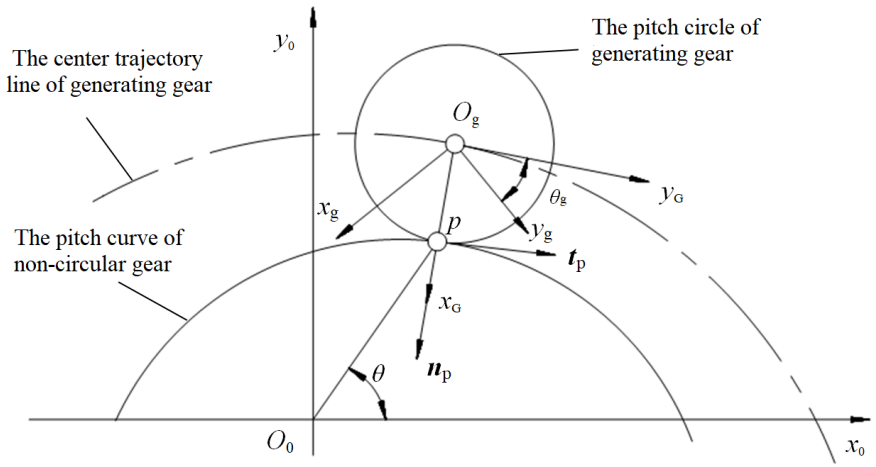

Fig. 2. *Coordinate transformation relationship during the production of NCG*

centre of the generating gear is the point of the radius of the normal gear shaper cutter. Using vector coordinate transformation, the unit vector of the three coordinate axes of the coordinate system S_p can be expressed as:

$$\begin{cases} \mathbf{i}_p(\theta) = \mathbf{n}_p(\theta) \\ \mathbf{j}_p(\theta) = \mathbf{t}_p(\theta) \\ \mathbf{k}_p(\theta) = [0\ 0\ 1]^T \end{cases}. \tag{2}$$

The unit vector of the three axes of coordinate system S_0 can be expressed as:

$$\begin{cases} \mathbf{i}_0 = [1\ 0\ 0]^T \\ \mathbf{j}_0 = [0\ 1\ 0]^T \\ \mathbf{k}_0 = [0\ 0\ 1]^T \end{cases}. \tag{3}$$

The coordinate transformation relationship between coordinate system S_G and coordinate system S_0 is as follows:

$$\mathbf{M}_{0G}(\theta) = \begin{bmatrix} \mathbf{n}_{p0} & \mathbf{t}_{p0} & 0 & \mathbf{r}_{og\,0} \\ \mathbf{n}_{p1} & \mathbf{t}_{p1} & 0 & \mathbf{r}_{og\,1} \\ 0 & 0 & 1 & 0 \\ 0 & 0 & 0 & 1 \end{bmatrix}. \tag{4}$$

(3) Gear shaper cutter coordinate system $S_g(O_g{-}x_g y_g z_g)$. In Fig. 2, the angle at which the relative coordinate system S_p rotates is the angle of rotation of the gear shaping cutter, which can be calculated based on the pure rolling relationship of the pitch curve using the following equation:

$$\theta_g = \frac{S_{pg}(\theta)}{r_{gp}} = \frac{\int_0^\theta \left| \mathrm{d}r_p(\theta)/\mathrm{d}(\theta) \right| \mathrm{d}(\theta)}{r_{gp}}, \tag{5}$$

where $S_{pg}(\theta)$ represents the arc length of the NCG pitch curve from the starting position to the current position. The coordinate transformation from the slotting cutter coordinate system S_g to the relative coordinate system S_p can be obtained as:

$$\mathbf{M}_{Gg}(\theta_g) = \begin{bmatrix} \cos\theta_g & \sin\theta_g & 0 & 0 \\ -\sin\theta_g & \cos\theta_g & 0 & 0 \\ 0 & 0 & 1 & 0 \\ 0 & 0 & 0 & 1 \end{bmatrix}. \tag{6}$$

According to Eqs. (4) and (6), the coordinate transformation from the gear shaper cutter coordinate system to the NCG coordinate system can be obtained as follows:

$$\mathbf{M}_{0g}(\theta) = \mathbf{M}_{0G}(\theta)\mathbf{M}_{Gg}(\theta_g). \tag{7}$$

Based on the analysis of gear-cutting tools according to the above generation motion, the tooth profile of NCG can be obtained. By transforming the tooth surface of the generation wheel into the gear coordinate system, the envelope equation of NCG can be obtained as follows:

$$\mathbf{R}_{Eg}(\theta, u, v) = \mathbf{M}_{0g}(\theta)\mathbf{R}_g(u, v). \tag{8}$$

The boundary of Eq. (8) is the tooth profile surface of an NCG, and its meshing equation is usually:

$$\mathbf{M}_{0g}(\theta)\mathbf{n}_{rg}(u, v) \cdot v_g = 0. \tag{9}$$

Due to the fixed gear coordinate system S_0, the relative velocity of the meshing point is the velocity of that point in the production wheel coordinate system. The motion of the auxiliary coordinate system S_G along the NCG pitch curve and the motion of the generative gear can be combined to form the relative velocity at the meshing point, so the relative velocity is:

$$\mathbf{v}_g(\theta,u,v)=\mathbf{t}_p(\theta)+\left[0 \quad 0 \quad \mathrm{d}\theta_g/\mathrm{d}\theta\right]^T\times\mathbf{R}_g(u,v). \quad (10)$$

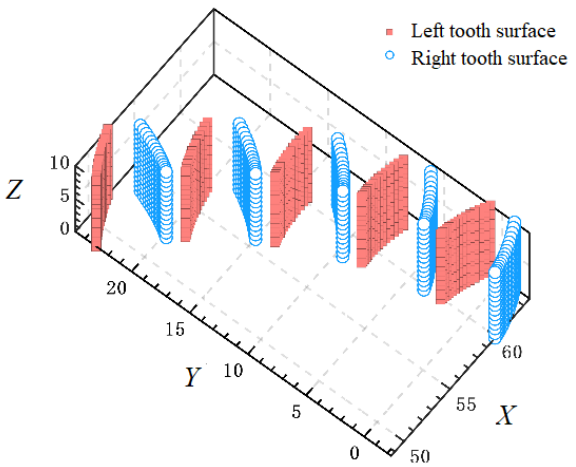

Fig. 3. *The partial digital tooth surface of the NCG*

By substituting Eq. (10) into the meshing Eq. (9), the instantaneous meshing line between the NCG and the generating gear at any time can be solved, thus forming the tooth profile of the NCG. The digital tooth surface of the NCG is established using Eq. (10), as shown in Fig. 3.

2 TRANSMISSION ERROR MODEL OF NEW W-W TYPE NCPGT

3.1 The Transmission Error Model of NCG Based on Meshing Line Increment Method

The transmission error of a gear transmission system is the main factor affecting its transmission performance and accuracy. Transmission errors caused by excitation parameters such as eccentricity error, time-varying backlash, and load are all dynamic transmission errors. The main idea of the incremental meshing method is to equate the centre distance error and eccentricity error to the instantaneous meshing line of the gear, and convert the increment of the meshing line of the driving gear and the driven gear under different turns into the angle of the driven gear, thus obtaining the transmission error of the driving gear under different turns.

In some cases, an NCG pair will be required to achieve reciprocating motion. Because the rotation centre of NCG is not at its geometric centre, there is an eccentricity error. The difference between the various tooth profiles of NCG results in a more pronounced excitation of transmission errors by the backlash between the teeth. There may be some differences in transmission between clockwise and counterclockwise rotation. Therefore, the meshing line increment of the driving and driven gears under different direction of rotation is considered in the analysis.

Figs. 4 and 5 show the transmission error analysis models of NCG pair established by the incremental meshing line method after considering the comprehensive eccentricity error and driving gear direction of rotation. Figs. 4a and b show the driving gear meshing line increment and driven gear meshing line increment when the driving gear

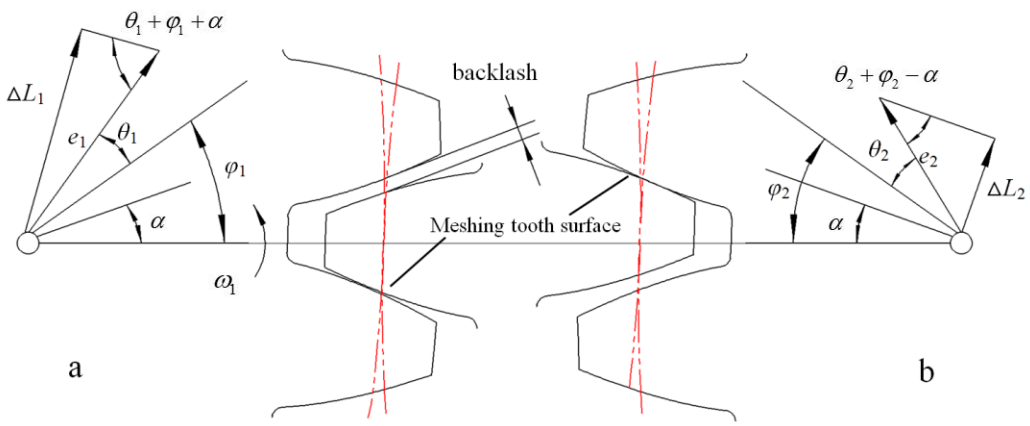

Fig. 4. *Calculation model of meshing line increment when driving gear rotates counterclockwise*

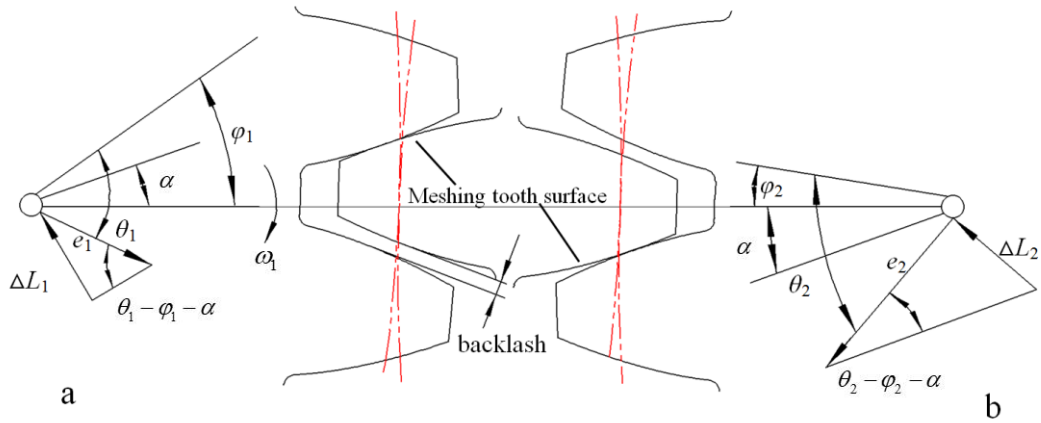

Fig. 5. *Calculation model of meshing line increment when driving gear rotates clockwise*

rotates counterclockwise, and Figs. 5a and b show the driving gear meshing line increment and driven gear meshing line increment when the driving gear rotates clockwise. Combined with Figs. 4 and 5, it can be determined that the increment of meshing line of driving gear and driven gears under two kinds of direction of rotation are:

$$\Delta L_1 = \mathrm{e}_1 \sin(\theta_1 \pm \varphi_1 + \alpha), \tag{11}$$

$$\Delta L_2 = \mathrm{e}_2 \sin(\theta_2 \pm \varphi_2 - \alpha), \tag{12}$$

where e_1 and e_2 are the eccentricity errors of the driving and driven gears, respectively. θ_1 and θ_2 are the rotation angles of the driving and driven gears, respectively. φ_1 and φ_2 are the initial phase angles of the driving and driven gears, respectively. ΔL_1 and ΔL_2 are the meshing line increments of the driving and driven gears, respectively. α is the pressure angle.

At the initial time, the increment of the meshing line of the driving and driven gears caused by the eccentricity error is as follows:

$$\Delta L_{10} = \mathrm{e}_1 \sin(\pm\varphi_1 + \alpha), \tag{13}$$

$$\Delta L_{20} = \mathrm{e}_2 \sin(\pm\varphi_2 - \alpha). \tag{14}$$

According to the meshing line increment method, when the driving gear rotates counterclockwise and clockwise, the theoretical no-load transmission error can be obtained as follows:

$$\begin{aligned}\Delta\varphi_{\mathrm{n}} = \frac{180}{\pi r\cos\alpha}\times[&\mathrm{e}_1\sin(\theta_1+\varphi_1+\alpha)\\ &+\mathrm{e}_2\sin(\theta_2+\varphi_2-\alpha)\\ &-\mathrm{e}_1\sin(\varphi_1+\alpha)\\ &-\mathrm{e}_2\sin(\varphi_2-\alpha)],\end{aligned} \tag{15}$$

$$\begin{aligned}\Delta\varphi_{\mathrm{s}} = \frac{180}{\pi r\cos\alpha}\times[&\mathrm{e}_1\sin(\theta_1-\varphi_1+\alpha)\\ &+\mathrm{e}_2\sin(\theta_2-\varphi_2-\alpha)\\ &-\mathrm{e}_1\sin(-\varphi_1+\alpha)\\ &-\mathrm{e}_2\sin(-\varphi_2-\alpha)].\end{aligned} \tag{16}$$

3.2 Establishment of Transmission Error Model of New W-W type NCPGT

A W-W type NCPGT consists of two externally engaged NCGs, and its structural principle is shown in Fig. 6, where 1, 2, 3 and 4 are NCGs. The NCG 1 and 4 are fixed, and H is a tie rod. The power is input from I, and the NCG 4 is driven to rotate by the rotation of the tie rod H, and the final power is output from NCG 4.

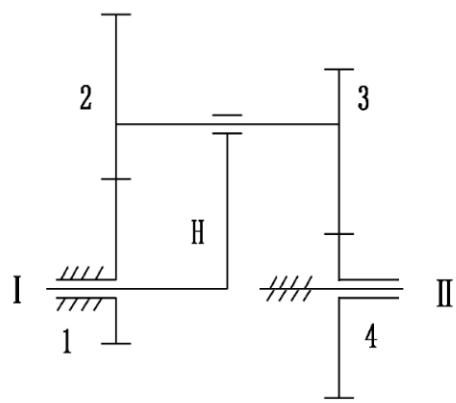

Fig. 6. *Schematic diagram of W-W type NCPGT mechanism*

Practice shows that the difference between the tooth profiles of NCGs leads to a certain vibration

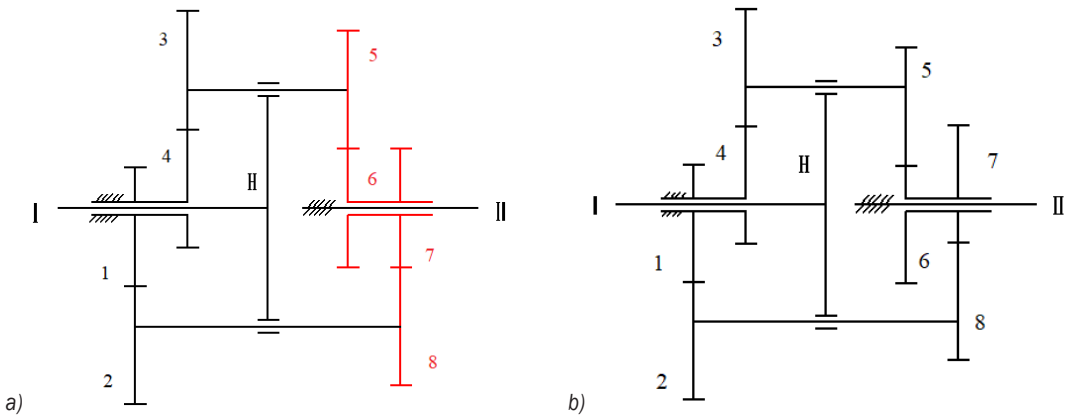

Fig. 7. *Schematic diagram of new W-W type NCPGT mechanism: case A, and b) case B*

of W-W gear train during operation, and there is also a certain fluctuation in the torque at the output end [21], which is not allowed for high-precision gear transmission systems. Therefore, on the basis of the traditional W-W gear train, this paper proposes two new combinations as shown in Fig. 7. Case A is composed of two externally engaged NCGs and two externally engaged cylindrical gears. In Fig.7a, 1, 2, 3 and 4 are NCGs, and 5, 6, 7 and 8 are cylindrical gears. Case B consists of four externally engaged NCGs. The new W-W type NCPGT formed by the above combination can achieve power balance and stable torque at the output end. The design parameters of NCGs are shown in Table 1.

Table 1. *The design parameters of NCGs*

	Cylindrical gear	NCG
Modulus [mm]	3.5	3
Tooth number	42	47
Eccentricity (k)	0	0.3287
Tooth width [mm]	30	30
Center distance [mm]	150	150
Pressure angle [°]	20	20 (Pitch line)
Pitch curve equation		$r(\theta)=\frac{64.667}{1-0.3287\cos\theta}$

To further clarify the engagement between gears, the two gear trains in Fig. 7 are simplified as shown in Fig. 8, where the red line represents Case A. In Fig. 8, the engagement of gears in Cases A and B is as follows: in Case A, the power input drives NCGs 2 and 3 to rotate by the tie rods at the axle holes of NCGs 1 and 4, and NCGs 1 and 4 are fixed. At the same time, the cylindrical gears 5 and 8 mesh with the cylindrical gears 6 and 7 respectively, and then the power is output by the sleeves of the shaft holes of the cylindrical gears 6 and 7. For Case B, only cylindrical gears 5 to 8 are replaced with NCGs, and its transmission mechanism is consistent with Case A.

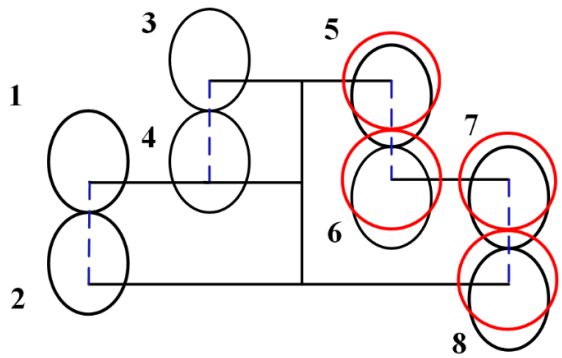

Fig. 8. *Schematic diagram of two types of NCPTG simplification*

The transmission error of a gear transmission system is the main factor affecting its transmission performance. During the meshing process of the NCG pair, due to the different tooth profiles, a certain displacement difference will be generated in the direction of the meshing line of the driving and driven gears [22] and [23], that is, transmission error. Most NCG transmission systems can realize quick return motion; at this time, its rotation centre is not at its geometric centre, thus involving eccentric errors. Therefore, the NCG in Cases A and B proposed in this paper also has eccentric errors. In view of the key role and special requirements of NCPGT in transmission, it is more practical to analyse the transmission error of an NCG transmission system under eccentric error. Based on the incremental meshing line method [23] to [25] and Eqs. (15) and (16), the transmission error models of the two cases proposed in this paper are established respectively. The general formula of

transmission error of each gear pair in Cases A and B is:

$$\Delta_{ij} = \frac{180}{\pi r_{jb} \cos\alpha_j}\left[e_i \sin\left(\theta_i + \varphi_i + \alpha_i\right) + e_j \sin\left(\theta_j + \varphi_j - \alpha_j\right) - e_i \sin\left(\varphi_i + \alpha_i\right) - e_j \sin\left(\varphi_j - \alpha_j\right)\right], \quad (i = 1,3,5,7 \quad j = 2,4,6,8), \tag{17}$$

where e is the eccentricity error. θ is the rotation angle. φ is the initial phase angle.

Therefore, the transmission errors of Case A and Case B are respectively:

$$TE_{\text{CaseA}} = \Delta_{\text{NCG12}} + \Delta_{\text{NCG34}} + \Delta_{\text{NCG56}} + \Delta_{\text{NCG78}}, \tag{18}$$

$$TE_{\text{CaseB}} = \Delta_{\text{NCG12}} + \Delta_{\text{NCG34}} + \Delta_{\text{CG56}} + \Delta_{\text{CG78}}. \tag{19}$$

Through the above mathematical model of transmission error, the transmission error distribution law of Cases A and B can be obtained under different design parameters, and the respective advantages of the two NCPGT can be determined through transmission error.

3.3 Comparative Analysis of Transmission Performance of New W-W-Type NCPGT

As the core component of the pumping unit, the transmission performance of the reversing device directly affects the quality and efficiency of the pumping unit. Therefore, it is necessary to systematically analyse the transmission performance of the reversing device of the proposed two NCPGTs. For the new W-W type NCPGT, this paper mainly compares and analyses the transmission error, output swing angle, angular velocity, kinetic energy and angular momentum to determine the optimal combination form. In Fig. 9, the transmission errors of Case A and Case B show a periodic change trend. As the NCG has eccentricity, the transmission error of the gear teeth under eccentric excitation has a cumulative effect. In contrast, the transmission errors of Case A are smaller, which indicates that the new W-W type NCPTG composed of NCGs and cylindrical gears has more advantages for high-precision transmission.

Figs. 10 and 11 show the variation trend of the transmission error of the NCPGT corresponding to Cases A and B with the eccentricity (k). With the increase of eccentricity, the transmission errors of the cases show an increasing trend. However, the transmission error in Case B increases more significantly. For the reversing device of a pumping unit, the transmission error is directly related to its up and down strokes, and excessive transmission error will lead to increased energy loss during the up and down strokes of the pumping unit. Therefore, Case A has better transmission performance based on transmission error analysis.

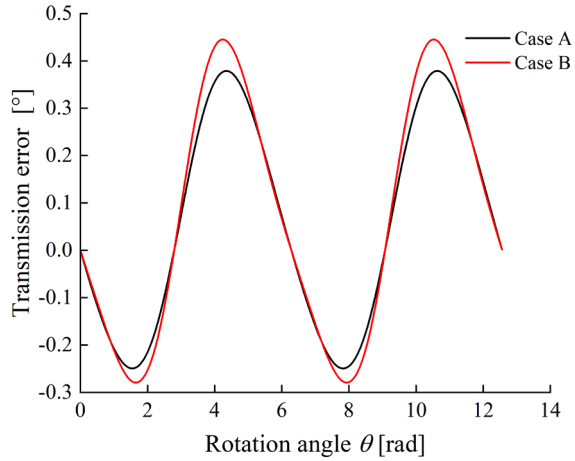

Fig. 9. *Transmission error distribution law of two cases*

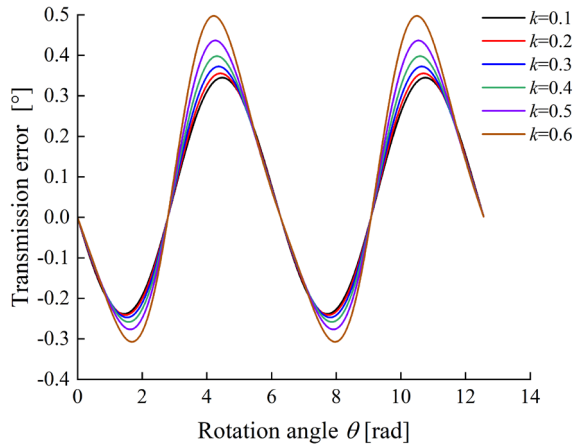

Fig. 10. *Variation trend of NCPGT transmission error corresponding to Case A with eccentricity*

To verify the above conclusions, a virtual prototype model (as shown in Fig. 12) was established for Cases A and B, respectively, and the working condition parameters consistent with the actual working condition of the pumping unit were set. By solving the model, the change laws of the contact force, frequency spectrum, output swing angle, angular velocity, kinetic energy, and angular momentum of the NCPGT corresponding to Cases A and B were obtained, respectively.

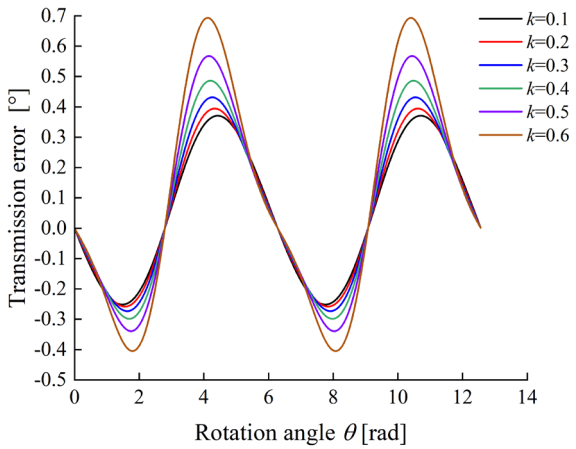

Fig. 11. *Variation trend of NCPGT transmission error corresponding to Case B with eccentricity*

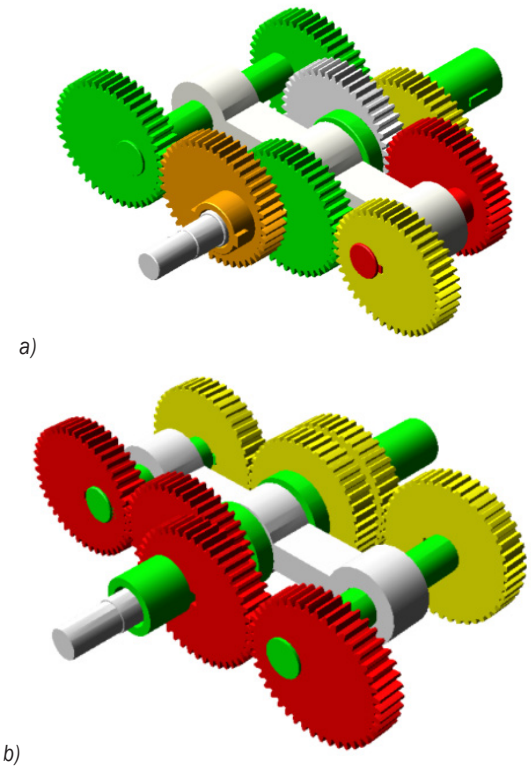

Fig. 12. *Virtual prototype model: a) Case A, b) Case B*

To demonstrate the differences between the original gear group and the added gear group, we conducted model validation to verify the rationality of the model proposed in this article. Fig. 13 shows the dynamic meshing force and frequency spectrum distribution of a) the original gear set (Fig. 6), (b) Case B, and (c) Case A. The original gear model has multiple peaks in the meshing force amplitude due to power imbalance and inertia force, which will exacerbate the impact and torque fluctuations of the system. In the model corresponding to Case B, the peak meshing force is mainly concentrated at the turning point of the gear train, which is around 0.72 seconds and 1.44 seconds. From a frequency perspective, it is mainly concentrated in the low-frequency range within 200 Hz. Compared to Case B, the model responding to Case A shows a decrease in the peak meshing force from 22 N to 18 N, and the change in meshing force during gear meshing is more uniform. Furthermore, the peak value tens to expand to both sides during the turning of the gear train. The system response frequency has also been wider, expanding from 200 Hz to 400 Hz. In Fig. 13c, there are many sub-harmonics with the same pattern in the distribution of the meshing force spectrum. Due to the addition of cylindrical gear pairs in the gear train, torque fluctuations in the initial stage of system dynamic balance will inevitably cause system vibration, which is necessary to reduce torque fluctuations in the initial stage of the system. To

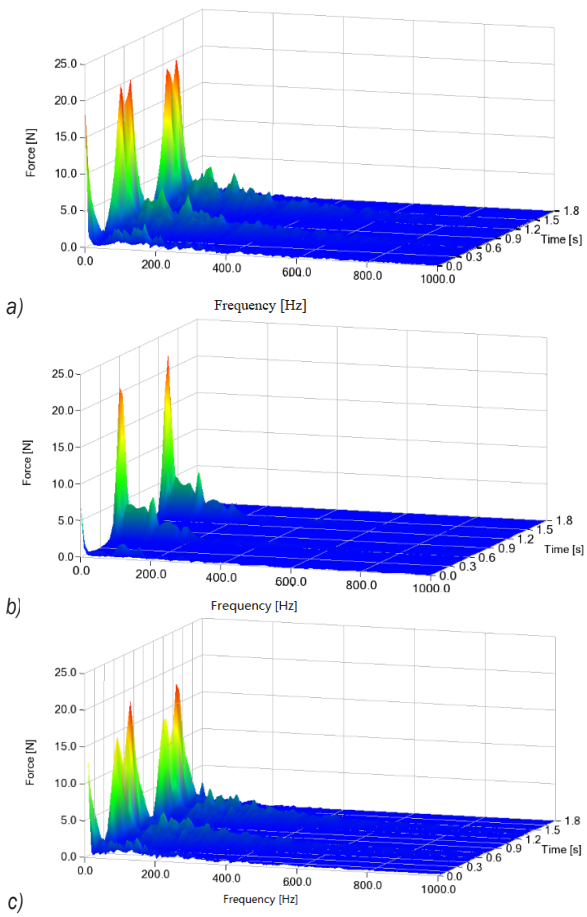

Fig. 13. *The distribution pattern of dynamic meshing force and spectral; a) the original gear set, b) Case B, and c) Case A*

summarize, compared with the above two schemes, the dynamic meshing force in Case A is reduced and the distribution is more uniform and gentle, which indicates that Case A has better motion characteristics and spectral distribution patterns.

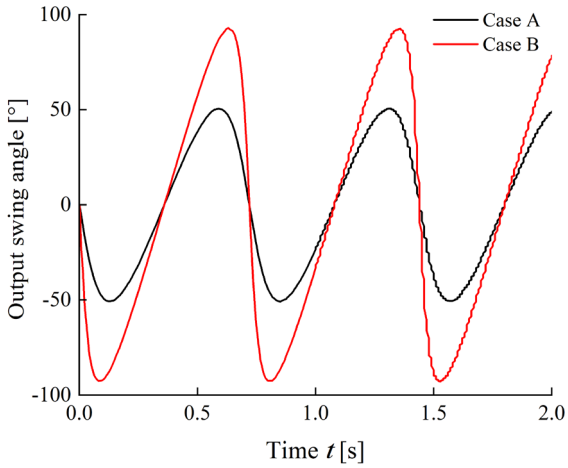

Fig. 14. *Comparison and analysis of output swing angle of two cases*

In Fig. 14, the output swing angle of Cases A and B shows a periodic change trend. The amplitude of the output swing angle corresponding to Case B is larger, but the time interval between the extreme values of the output swing angle is longer. For pumping units, a large output swing angle means that a longer stroke can be achieved, which is expected in the pumping process and is of great significance for improving the working efficiency of pumping units. However, the curve in Case B fluctuates greatly, while Case A can reduce the vibration caused by NCG pair engagement on the basis of achieving stable power because of the introduction of cylindrical gears to participate in planetary gear train engagement. The vibration phenomenon should be avoided as much as possible during the working process of the pumping unit, and the output swing angle can be adjusted by the sprocket system at the output end of the reversing device of the pumping unit. In contrast, the stability of the system is more important.

Figs. 15 to 17 show the angular velocity, kinetic energy and angular momentum curves of Cases A and B respectively. The negative value appears in Fig. 14, which is due to the preset clockwise rotation as a square during multi body dynamics simulation. When the output end of NCPGT rotates counterclockwise, a negative value will appear. In Fig. 15, Case B has great velocity fluctuation and impact during reversing, while Case A's angular velocity curve is

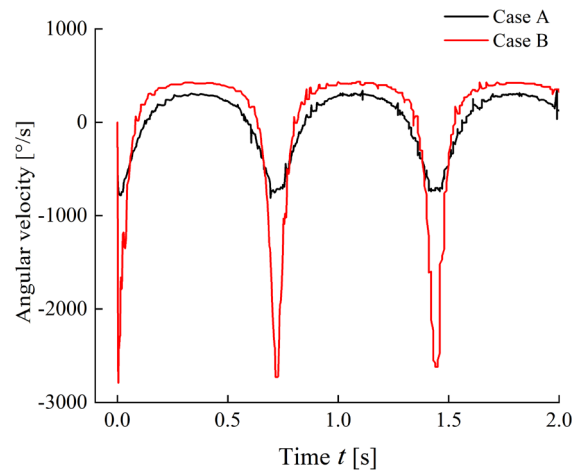

Fig. 15. *Comparison and analysis of angular velocity of two cases*

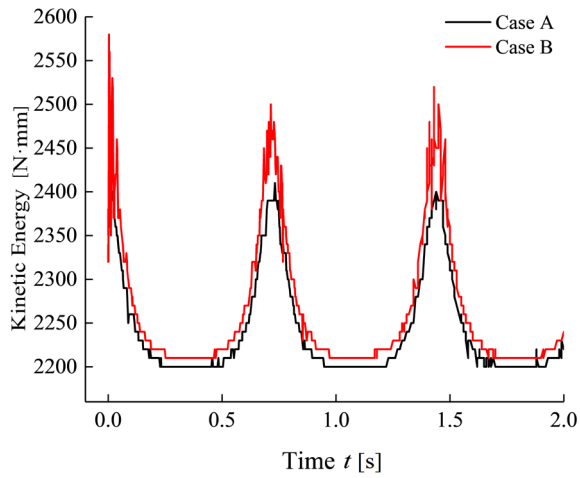

Fig. 16. *Comparison and analysis of kinetic energy of two cases*

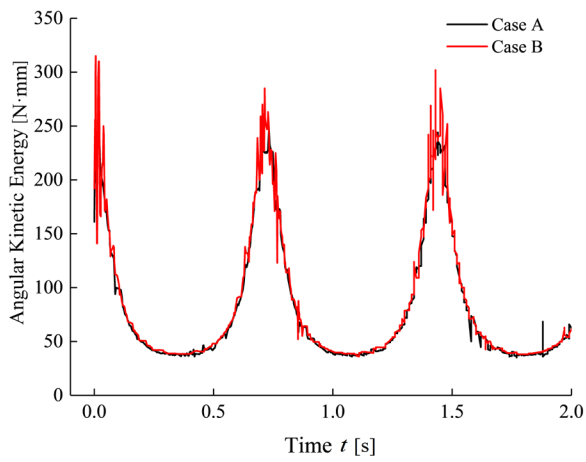

Fig. 17. *Comparison and analysis of angular kinetic energy of two cases*

more periodic. In Figs. 16 and 17, although Cases A and B have the same distribution law, the impact and fluctuation of Case B are larger. It is indicated that within a certain range, the impact of NCG gear pairs on the transmission performance of the system can be reduced by introducing cylindrical gears, thereby reducing the vibration and impact of the system. The above analysis further shows that the NCPGT formed by the combination of NCG and cylindrical gear has better transmission performance, and also verifies the correctness of the transmission error analysis results. Therefore, the Case A scheme is adopted for the subsequent pumping unit reversing device.

3 TRANSMISSION TEST OF PUMPING UNIT REVERSING DEVICE

The idealized indoor test of sucker rod pumping unit is realized by building a test prototype with the same proportion as the actual pumping unit. The test prototype of the pumping unit is shown in Fig. 18. Its working principle is as follows: the motor inputs torque into the NCPGT reversing device of the pumping unit through belt transmission. The output shaft transmits the torque to the drum through the sprocket drive and finally completes the up and down stroke movement of the sucker rod through the connection between the steel wire rope wound on the drum and the simulation loading device. During the experiment, an MPS wire displacement sensor was used to detect the real-time displacement of the suspension point; The DYLY-102 tensile sensor is used to measure the suspension load. Finally, the indicator diagram is drawn based on the dynamic matching relationship between them.

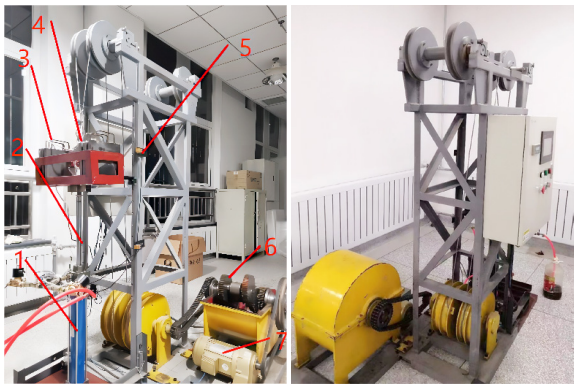

Fig. 18. *NCPGT reversing device pumping unit; 1 hydraulic cylinder, 2 sucker rod, 3 balance weight, 4 DYLY-102 tensile sensor, 5 MPS wire displacement sensor, 6 new w-w type NCPGT, and 7 variable frequency motor*

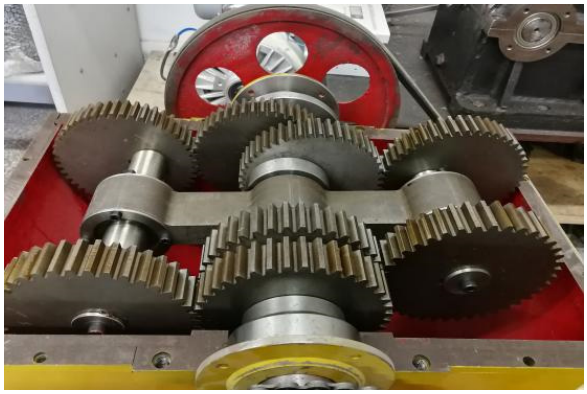

Fig. 19. *New W-W type NCPGT reversing device*

Fig. 19 shows the new W-W type NCPGT reversing device corresponding to Case A. The indicator diagram is an important indicator for evaluating the performance of the pumping unit **[26]**. A closed parallelogram can be formed by real-time collecting the corresponding data in a cycle of the suspension point load and displacement sensor, and then establishing a two-dimensional coordinate system with suspension point displacement and load as the horizontal axis and vertical axis respectively. However, due to the influence of complex environment, the measured indicator diagram curve often has certain fluctuations.

The balance weight and stroke times of sucker rod will affect the stability of pumping unit operation. During the test, the counterweight of the counterweight box and the motor frequency are given. The indicator diagrams of pumping units under different working conditions are obtained by dynamically adjusting the experimental data, as shown in Figs. 20 and 21.

In Fig. 20, the change of polished rod load during up and down strokes has great fluctuation. The reason is that the impact and vibration of the gear pair in the new W-W type NCPGT reversing device during meshing, and the load mismatch in the up and down strokes under the load frequency mode aggravates this situation.

Fig. 21 shows the indicator diagram of the pumping unit under three working conditions: load is 20 kN, and motor frequencies are 10 Hz, 15 Hz, and 20 Hz, respectively. There are obvious fluctuations at the starting point of the upstroke, which leads to a large impact at the starting point of the pumping unit. The reason is that the inertia of the sucker rod counterweight load is too large, and the pumping unit stroke is not dynamically adjusted. With further increase of the motor frequency, the polished rod load line obviously tends to be stable, showing a stable state, and there is basically no fluctuation. In the

process of the down stroke, the fluctuation amplitude of polished rod load decreases gradually and tends to be stable. It shows that the pumping unit has the best balance weight and pumping stroke, and adjusting the motor frequency is helpful to balance the polished rod load from the up and down strokes of the pumping rod. Therefore, increasing the motor frequency can effectively improve the performance of the pumping unit.

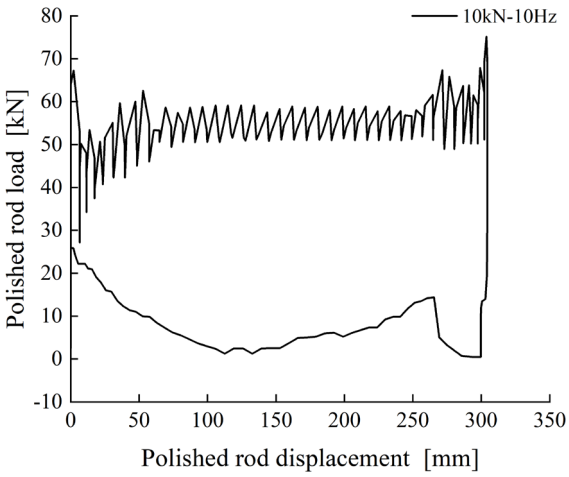

Fig. 20. *Indicator diagram of 10 kN load*

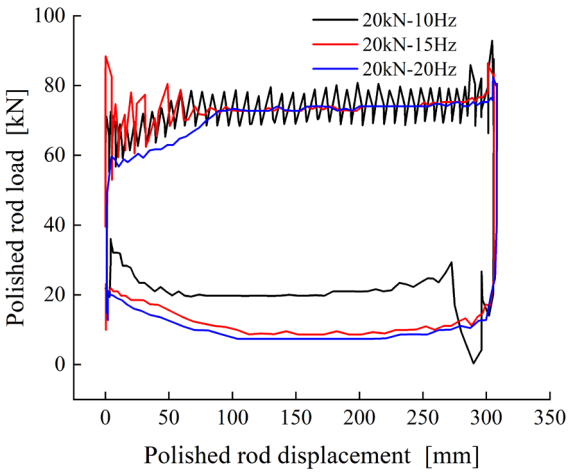

Fig. 21. *Variation trend of indicator diagram of pumping unit with motor frequency under 20 kN load*

Fig. 22 shows the indicator diagram of the pumping unit when the load is 30 kN and the motor frequencies are 15 Hz and 20 Hz, respectively. The polished rod load at the starting point and the end point of the down stroke of the pumping unit fluctuates slightly. The vibration of the polished rod load at the beginning of the upstroke has an obvious decreasing trend with the increase of the motor frequency, which indicates that increasing the motor frequency can significantly reduce the load impact at the upper and lower dead points of the pumping unit.

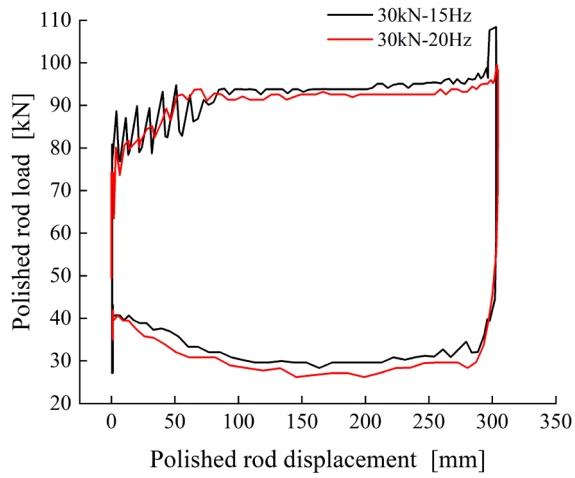

Fig. 22. *Variation trend of indicator diagram of pumping unit with motor frequency under 30 kN load*

Based on the comparison and analysis of indicator diagrams of several groups of different tests from Figs. 20 to 22, it is concluded that the pumping unit is the most stable when the load frequency matching mode of the pumping unit is 20 kN and 20 Hz. At this time, the pumping unit has the optimal balance weight and the optimal pumping unit stroke. Therefore, the above analysis shows that the load imbalance problem during the operation of the pumping unit can be alleviated by adjusting the matching between the load and the motor frequency. It can also reduce the impact and vibration caused by the reversing of the NCPGT reversing device, thereby improving the efficiency of the pumping unit and the service life of the reversing device.

4 CONCLUSIONS

This paper proposes two new combination methods for W-W type NCPGT. Based on the incremental meshing line method, the transmission error models are established respectively. The advantages of the two types of gear trains are judged by the contact force, frequency spectrum, transmission error, output swing angle, angular velocity, kinetic energy, and angular momentum. The correctness of the analysis is verified by the virtual prototype model. The new W-W type NCPGT, which is composed of NCGs and cylindrical gears, has better transmission performance. On this basis, the new W-W type NCPGT is applied to the reversing device of the drum pumping unit,

and the idealized rod production laboratory test is carried out. The indicator diagrams under different load frequency matching modes are obtained, and the optimal load frequency matching mode is 20kN-20Hz. The test results further show that adjusting the motor frequency can effectively achieve the dynamic load balance of the test pumping unit. The research results in this paper can lay a theoretical foundation for the industrial application and improvement of the transmission performance of NCPGT.

5 ACKNOWLEDGMENTS

The research was supported by the National Natural Science Foundation of China (Grant No.52265008), the Gansu Province Youth Science Foundation Project of China (Grant No. 23JRRA751), the Gansu Provincial Department of Education of China: Innovation Fund Project for University Teachers (Grant No. 2023A-021), the Open Fund of Hubei Key Laboratory of Mechanical Transmission and Manufacturing Engineering at Wuhan University of Science and Technology (Grant No. MTMEOF2023B01) and the Key Research and Development Program of Hubei Province of China (Grant No. 2021BAA202).

6 REFERENCES

[1] Dong, C.B., Liu, Y.P., Wei, Y.Q., Yun, B.B., Li, D.W., Dong, Z.Q. (2020). Analysis on meshing characteristics and transmission error of elliptic gears. *Mathematical Problems in Engineering*, vol. 2020, art. ID 2017218, **DOI:10.1155/2020/2017218**.

[2] Niu, R., Wang, G. (2020). Application of non-circular gear system in artillery system. *Fire Control & Command Control*, vol. 45, p. 102-104, **DOI:10.3969/j.issn.1002-0640.2020.02.020**. (in Chinese)

[3] Osiecki, L. (2019). New generation of the satellite hydraulic pumps. *Journal of Mechanical and Energy Engineering*, vol. 3, no. 4, p.309-314, **DOI:10.30464/JMEE.2019.3.4.309**.

[4] Ye, B., Wu, G., Yu, G., Jin, X., Sun, L. (2016). Optimized design and tests on rice potted seedling transplanting mechanism of planetary gear train with non-circular gears. *Transactions of the Chinese Society for Agricultural Machinery*, vol. 47, p. 68-73, **DOI:10.6041/j.issn.1000-1298.2016.11.009**. (in Chinese)

[5] Burrows, M., Sutton, G. (2013). Interacting gears synchronize propulsive leg movements in a jumping insect. *Science*, vol. 341, no. 6151, p. 1254-1256, **DOI:10.1126/science.1240284**.

[6] Addomine, M., Figliolini, G., Pennestri, E. (2018). A landmark in the history of non-circular gears design: The mechanical masterpiece of Dondi's astrarium. *Mechanism and Machine Theory*, vol. 122, p. 219-232, **DOI:10.1016/j.mechmachtheory.2017.12.027**.

[7] Xu, G., Chen, J., Zhao, H. (2018). Numerical calculation and experiment of coupled dynamics of the differential velocity vane pump driven by the hybrid higher-order Fourier non-circular gears. *Journal of Thermal Science*, vol. 27, p. 285-293, **DOI:10.1007/s11630-018-1010-7**.

[8] Zhao, Y., He, C. (2022). Matching between mechanics and thermodynamics among 4 individual strokes in a 4-stroke engine by non-circular gear mechanism. *Journal of Central South University*, vol. 29, p. 2112-2126, **DOI:10.1007/s11771-022-5024-7**.

[9] Yokoyama, Y., Ogawa, K., Kurebayashi, S. (1973). Studies on the noncircular planetary gear mechanisms. *Japan Society of Mechanical Engineers Proceedings*, vol. 39, no. 317, p. 393-403, **DOI:10.1299/kikai1938.39.393**. (in Japanese)

[10] Mundo, D. (2006). Geometric design of a planetary gear train with non-circular gears. *Mechanism and Machine Theory*, vol. 41, no. 4, p. 456-472, **DOI:10.1016/j.mechmachtheory.2005.06.003**.

[11] Ye, B., Yi, W., Yu, G., Gao, Y., Zhao, X. (2017). Optimization design and test of rice plug seedling transplanting mechanism of planetary gear train with incomplete eccentric circular gear and non-circular gears. *International Journal of Agricultural and Biological Engineering*, vol. 10, no. 6, p. 43-55, **DOI:10.25165/j.ijabe.20171006.2712**.

[12] Zhao, X., Chu, M., Ma, X., Dai, L., Ye, B., Chen, J. (2018). Research on design method of non-circular planetary gear train transplanting mechanism based on precise poses and trajectory optimization. *Advances in Mechanical Engineering*, vol. 10, no. 12, p. 1-12, **DOI:10.1177/1687814018814368**.

[13] Sun, L., Shen, J., Zhou, Y., et al. (2019). Design of non-circular gear linkage combination driving type vegetable pot seedling transplanting mechanism. *Transactions of the Chinese Society for Agricultural Machinery*, vol. 35, pp. 26-33, DOI:**10.11975/j.issn.1002-6819.2019.10.004**. (in Chinese)

[14] Sun, L., Hu, Y., Xing, Z. et al. (2020). Motion synthesis of rotary pot seedling transplanting mechanism based on approximate multi-pose. *Transactions of the Chinese Society for Agricultural Machinery*, vol. 51, p.103-111, **DOI:10.6041/jissn.1000-1298.2020.12.011**. (in Chinese)

[15] Zhao, X., Ye, J., Chu, M., Dai, L., Chen, J. (2020). Automatic scallion seedling feeding mechanism with an asymmetrical high-order transmission gear train. *Chinese Journal of Mechanical Engineering*, vol. 33, no. 10, p. 1-14, **DOI:10.1186/s10033-020-0432-9**.

[16] Ye, B., Zeng, G., Deng, B., Yang, C., Liu, J., Yu, G. (2020). Design and tests of a rotary plug seedling pick-up mechanism for vegetable automatic transplanter. *International Journal of Agricultural and Biological Engineering*, vol. 13, no. 3, p.70-78, **DOI:10.25165/j.ijabe.20201303.5647**.

[17] Yu, Y., Liu, J., Ye, B., Jin, X., Sun, L., Tong, J. (2019). Design and experimental research on seedling pick-up mechanism of planetary gear train with combined non-circular gear transmission. *Chinese Journal of Mechanical Engineering*, vol. 32, no. 49, p. 1-13, **DOI:10.1186/s10033-019-0357-3**.

[18] Wang, L., Sun, L., Xu, Y., Yu G.H., Zhang, W., Zheng, J. (2021). Design method of transplanting mechanism of planetary gear train based on spatial trajectory. *Transactions of the Chinese Society of Agricultural Machinery*, vol. 52, p. 51-59, **DOI:10.6041/j.issn.1000-1298.2021.07.005**. (in Chinese)

[19] Y. Liu, X. Fu, Y. Wei, Li, D.W. (2021). Parametric design and motion simulation analysis of Non-circular gear planetary gear

train. *Journal of Mechanical Transmission*, vol. 45, p. 70-75, **DOI:10.16578/j.issn.1004.2539.2021.08.010**. (in Chinese)

[20] Lin, C., Xia, X., Li, P. (2018). Geometric design and kinematics analysis of coplanar double internal meshing non-circular planetary gear train. *Advances in Mechanical Engineering*, vol. 10, no. 12, p. 1-12, **DOI:10.1177/1687814018818910**.

[21] Dong, C., Liu, Y., Zhao, G. (2021). A method for calculating elliptic gear transmission efficiency based on transmission experiment. *Strojniški vestnik - Journal of Mechanical Engineering*, vol. 67, no. 11, p. 557-569, **DOI:10.5545/sv-jme.2021.7318**.

[22] Margielewicz, J., Gąska, D., Litak, G. (2019). Modelling of the gear backlash. *Nonlinear Dynamics*, vol. 97, p.355-368, **DOI:10.1007/s11071-019-04973-z**.

[23] Dong, C., Liu, Y. (2022). Experimental study on transmission error and dynamic backlash of elliptic gear transmission system. *Proceedings of the Institution of Mechanical Engineers, Part K: Journal of Multi-body Dynamics*, vol. 236, no. 1, p. 130-139, **DOI:10.1177/14644193221077494**.

[24] Zou, S., L. Yu, G. Wang, et al. (2017). Research on the dynamic transmission error of a spur gear pair with eccentricities by finite element method. *Mechanism and Machineary Theory*, Vol. 109, pp. 1-13, **DOI:10.1016/j.mechmachtheory.2016.11.006**.

[25] Wang, G., Zhu, D., Zou, S., Jing, Y., Tian, X. (2022). Simulation and experimental research on electrical control anti-backlash based on a novel type of variable tooth thickness involute gear pair. *Strojniški vestnik - Journal of Mechanical Engineering*, vol. 68, no. 2, p. 126-140, **DOI:10.5545/sv-jme.2021.7452**.

[26] Yin, X., Du, Z., Wang, Y., Lu, S., Li, Y., Zhao, T. (2022). Analysis and experimental study of oil well indicator diagram based on electric parameter method. *Energy Reports*, vol. 8, supp. 4, p.732-745, **DOI:10.1016/j.egyr.2022.02.013**.